Signatures of a quantum Griffiths phase close to an electronic nematic quantum phase transition

Pascal Reiss,[1,*] David Graf,[2] Amir A. Haghighirad,[1,3] Thomas Vojta,[4] and Amalia I. Coldea[1,†]

[1] *Clarendon Laboratory, Department of Physics, University of Oxford, Oxford, UK*
[2] *National High Magnetic Field Laboratory, Florida State University, Tallahassee, FL, USA*
[3] *Institute for Quantum Materials and Technologies, Karlsruhe Institute of Technology, Karlsruhe, Germany*
[4] *Department of Physics, Missouri University of Science and Technology, Rolla, MO, USA*

(Dated: September 27, 2021)

In the vicinity of a quantum critical point, quenched disorder can lead to a quantum Griffiths phase, accompanied by an exotic power-law scaling with a continuously varying dynamical exponent that diverges in the zero-temperature limit. Here, we investigate a nematic quantum critical point in the iron-based superconductor $FeSe_{0.89}S_{0.11}$ using applied hydrostatic pressure. We report an unusual crossing of the magnetoresistivity isotherms in the non-superconducting normal state which features a continuously varying dynamical exponent over a large temperature range. We interpret our results in terms of a quantum Griffiths phase caused by nematic islands that result from the local distribution of Se and S atoms. At low temperatures, the Griffiths phase is masked by the emergence of a Fermi liquid phase due to a strong nematoelastic coupling and a Lifshitz transition that changes the topology of the Fermi surface.

Introduction A central characteristic of finite- and zero-temperature phase transitions is how the spatial and temporal correlation lengths evolve as the transition is approached. For clean and continuous phase transitions, scaling theory predicts power-law divergences of both correlation lengths as a function of control parameter, with the critical exponents reflecting the universality class. Moreover, the spatial and temporal correlation lengths are closely related by the dynamics of the system [1–4]. In the presence of quenched disorder, this relation may be lost. Quenched disorder is perfectly correlated in time, but can harbor a spatially varying order parameter. In this situation, a smeared phase transition can occur, where ordered islands form within a disordered bulk [5, 6]. Moreover, when order parameter fluctuations within the islands are non-negligible, a Griffiths phase can emerge which leads to continuously varying critical exponents as a function of temperature and control parameter, fundamentally different to clean systems [7–13].

Experimentally, quantum Griffiths phases have been identified in ferromagnetic alloys [14, 15], heavy-fermions [16, 17], the hidden-order phase of URu_2Si_2 [18], and superconducting thin films [19–22]. In the latter systems, sharp crossings of the magnetoresistivity isotherms emerged as a distinctive experimental signature [23–26]. A scaling analysis revealed a temperature-dependent critical exponent $z\nu$ that diverges in the low-temperature limit. This is a hallmark of a quantum Griffiths phase (ν is the critical correlation length exponent, and z the dynamical exponent) [8–13].

In this Letter, we report the experimental realization of an unconventional quantum Griffiths phase in a electronic nematic system. Specifically, we report the magnetoresistivity of the quasi-2D bulk superconductor $FeSe_{0.89}S_{0.11}$ when tuned to the vicinity of its zero-temperature nematic quantum critical point (QCP) using a hydrostatic pressure of 4.7 kbar (Fig. 1(a)) [27]. Only at the nematic QCP, the magnetoresistivity isotherms show a remarkably sharp crossing at about 30 T over nearly two decades in temperature up to 30 K. Scaling of the

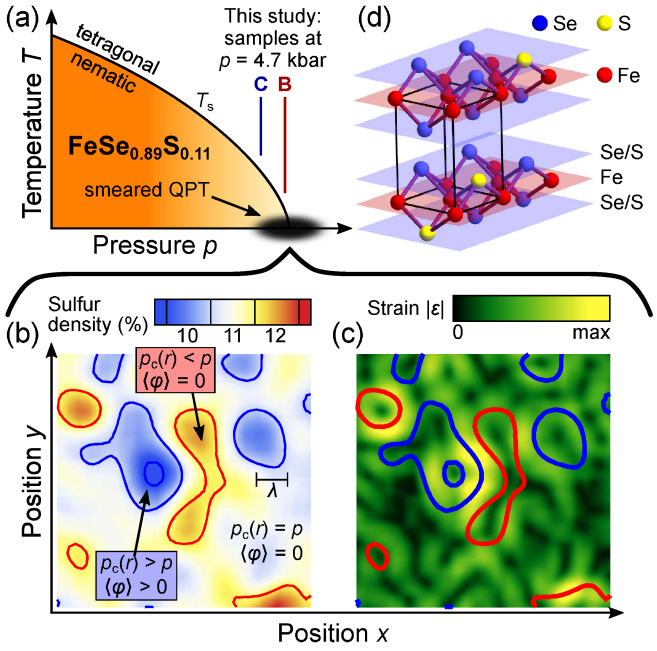

FIG. 1. (a) Pressure-temperature phase diagram and (d) crystal structure of $FeSe_{0.89}S_{0.11}$. The relative position of samples B and C under a pressure of $p = 4.7$ kbar are indicated by vertical lines. (b,c) The spatial distribution of small S atoms induces locally varying critical pressures $p_c(r)$ and random local strains. Close to the nematic quantum phase transition (QPT), this leads to the formation of nematic islands. The scale shows the experimental mean free path length λ [27].

magnetoresistivity yields a critical exponent $z\nu$ which increases by more than two orders of magnitude and diverges at low temperatures, in agreement with the quantum Griffiths scenario. This divergence is much stronger than previous reports of non-nematic systems where a comparatively modest enhancement of $z\nu$ was observed only. We argue that the Griffiths phase is induced by the local distribution of isoelectronic Se and S atoms that promote the formation of nematic islands in the vicinity of the nematic QCP, as shown in Fig. 1(b) and (c). Below a crossover temperature $T \approx 10\,\mathrm{K}$, the quantum Griffiths phase and the nematic QCP appear to be masked by an emergent non-zero energy scale which coincides with the re-entrance of Fermi liquid behavior attributed to a strong nematoelastic coupling, as well as a topological Lifshitz transition of the Fermi surface.

Methods Single crystal of $FeSe_{1-x}S_x$ with $x = 0.11$ sulfur substitution were grown using the $KCl/AlCl_3$ chemical vapour transport method as described elsewhere [28]. High-pressure, high-field measurements for samples B and C were carried out in the 45 T hybrid DC facility in Tallahassee. We used Daphne Oil 7575 as pressure medium which ensures hydrostatic conditions for much higher pressures than reported here, and we used the Ruby fluorescence shifts below 4 K to determine the pressure. Low-field measurements up to 13.5 T were carried out on sample A in a QuantumDesign PPMS in Oxford. Here, Daphne Oil 7373 was used, and the pressure was determined by the superconducting transition of tin. Samples were aligned with the magnetic field parallel to the crystallographic c axis to avoid breaking an in-plane symmetry. Transport measurements were performed using a standard 4 or 5 contact setup, using the AC LockIn technique with a low frequency $f \approx 20\,\mathrm{Hz}$, and a low excitation current $I_p = 1\,\mathrm{mA}$ within the (ab) plane.

Results Figure 2(a) and (b) show the temperature dependence of the magnetoresistivity of two different single crystals B and C of $FeSe_{0.89}S_{0.11}$ under a hydrostatic pressure of $p = 4.7\,\mathrm{kbar}$, which are in the immediate vicinity of their nematic QCPs ($p_c = 4.8(3)\,\mathrm{kbar}$ for sample B and $5.2(3)\,\mathrm{kbar}$ for sample C, respectively as shown in Fig. 1(a) and in the Supplemental Material (SM) [27, 29, 30]). All magnetoresistivity isotherms cross around a similar magnetic field, $\mu_0 H^\star \approx 28.6\,\mathrm{T}$ for sample B and 28.0 T for sample C, with similar resistivities $\rho^\star \approx 32\,\mu\Omega\,\mathrm{cm}$ and $34\,\mu\Omega\,\mathrm{cm}$, respectively. This crossing occurs over nearly two decades in temperature $0.3\,\mathrm{K} \lesssim T \lesssim 30\,\mathrm{K}$ and its significance becomes evident in the resistivity plots as a function of temperature in constant field, shown in Fig. 2(c). For $H < H^\star$, the resistivity follows a metallic-like behavior with $\partial\rho/\partial T > 0$ before the sample becomes superconducting below $T_c^{\mathrm{on}} \approx 10\,\mathrm{K}$ (Fig. 2(d)). Equivalently, the onset magnetic field, H_{c2}^{on}, between the superconducting and normal phases can be identified in magnetic fields smaller than $H^\star$ in Fig. 2(e) whose zero-temperature extrapolation coincides with $H^\star$ (Fig. 2(f)). Thus, the magnetoresistivity crossing occurs strictly within the non-superconducting normal phase for all finite temperatures ($H^\star > H_{c2}^{\mathrm{on}}(T)$), implying that this behavior describes the normal phase in the vicinity of the nematic QCP.

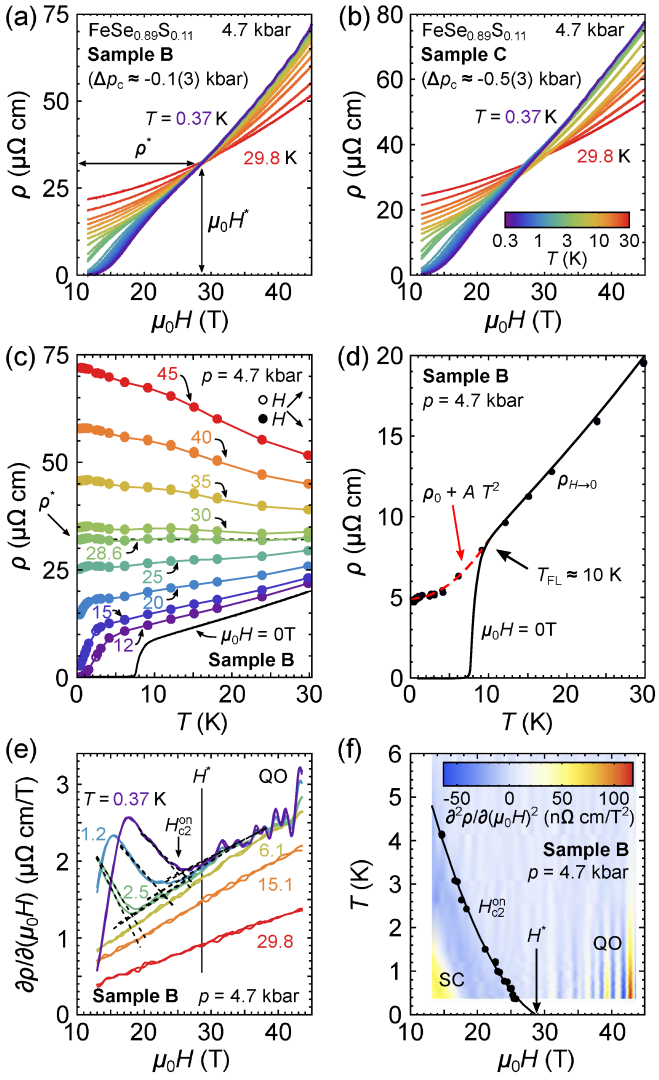

FIG. 2. (a,b) The isothermal magnetoresistivity of samples B and C at a pressure of $p = 4.7\,\mathrm{kbar}$ cross at $\mu_0 H^\star \approx 28\,\mathrm{T}$, $\rho^\star \approx 33\,\mu\Omega\,\mathrm{cm}$. Up and down sweeps show no hysteresis. The pressure difference in brackets represents the distance to the critical pressure (see Fig. 1(a) and in the SM [29]). (c) The same data as in panel (a), but as a function of temperature in fixed field. (d) The actual and extrapolated zero-field resistivities, $\rho(T)$ (solid line) and $\rho_{H\to 0}$ (points, see the SM [29]). Error bars are smaller than the symbol size. The red dashed line is a fit to Fermi liquid behavior ($\rho_0 \approx 4.9\,\mu\Omega\,\mathrm{cm}$, $A \approx 0.036\,\mu\Omega\,\mathrm{cm/K^2}$). (e) The first derivative reveals the onset of superconductivity, indicated by arrows. Large quantum oscillations (QO) can be seen for $H > H^\star$. (f) The extrapolation of the superconducting (SC) onset coincides with $H^\star$ only at $T = 0$. All reported data are measured at $p = 4.7\,\mathrm{kbar}$.

In high magnetic fields above $H^\star$, the resistivity shows

insulating-like behavior ($\partial\rho/\partial T < 0$), before it saturates below $T \approx 2\,\mathrm{K}$ (Fig. 2(c)), similar to previous reports [31]. Despite this insulating-like behavior, the large magnetoresistivity is a feature of the metallic, compensated multi-band system $FeSe_{1-x}S_x$ [31–33]. Quantum oscillations are visible for temperatures below $\approx 5\,\mathrm{K}$ (Fig. 2(e)), demonstrating the existence of a Fermi surface and highlighting the high quality of the samples [27, 34]. A two-band analysis of the magnetoresistivity allows us to extrapolate the zero-field resistivity from high magnetic fields [29], which indicate Fermi liquid behavior below a crossover temperature $T_{\mathrm{FL}} \approx 10\,\mathrm{K}$, shown in Fig. 2(d) [27, 31]. The orbitally averaged effective masses from quantum oscillations show non-divergent electronic correlations in the vicinity of the nematic QCP, as discussed in detail in Ref. 27, likely due to a coupling between the nematic order parameter and the lattice [35–38].

Next, we use a prototypical power-law scaling ansatz to describe the magnetoresistivity of $FeSe_{0.89}S_{0.11}$, previously applied in thin-film materials, including dirty films of FeSe [19–26]. In d dimensions, the scaling is given by

$$\rho(H,T)/\rho^\star = T^{(2-d)/z} f\left(\mu_0|H - H^\star|/T^{1/z\nu}\right) \qquad (1)$$

with $f(0) = 1$ and the critical exponent $z\nu$ [39]. Clearly, a crossing of the magnetoresistivity isotherms at a finite $\rho^\star$ is only possible for a two-dimensional system. Indeed, $FeSe_{1-x}S_x$ have strongly two-dimensional electronic and superconducting properties [27, 33, 40–43].

In the case of a typical QCP, $z\nu$ is a constant given by the appropriate universality class, which would lead to a constant slope in Fig. 3(a) (see also the SM [29]). This is evidently not the case here where we identify a power-law dependence of $z\nu(T) \sim T^\alpha$, with non-universal exponents $\alpha \approx -1.5$ for sample B and ≈ -1.0 for sample C, as shown in Fig. 3(b). Using this extracted $z\nu(T)$, all magnetoresistivity data collapse onto a single curve for both samples, reflecting the form of the scaling function f, shown in Fig. 3(c). Deviations for this scaling only occur for the superconducting transition at lowest fields and temperatures, and at the highest temperatures and fields. These deviations indicate the limits of the scaling relation, as shown in the SM [29].

This scaling analysis reveals an interesting and unexpected feature. While a zero-temperature divergence of the effective critical exponent $z\nu(T)$ is a key signature of quantum Griffiths phases, the power-law divergence observed here is much stronger than the logarithmic ('activated') divergence predicted within the infinite-randomness criticality scenario [13, 21, 29], as shown in Fig. 3(b). In fact, a power-law divergence of $z\nu(T)$ is incompatible with the presence of a typical QCP because the temperature term $T^{1/z\nu(T)}$ in Eq. 1 remains finite for $T \to 0$, which implies the persistence of a non-zero energy scale at lowest temperatures. Interestingly, we find that $z\nu$ deviates from the activated behavior dependence

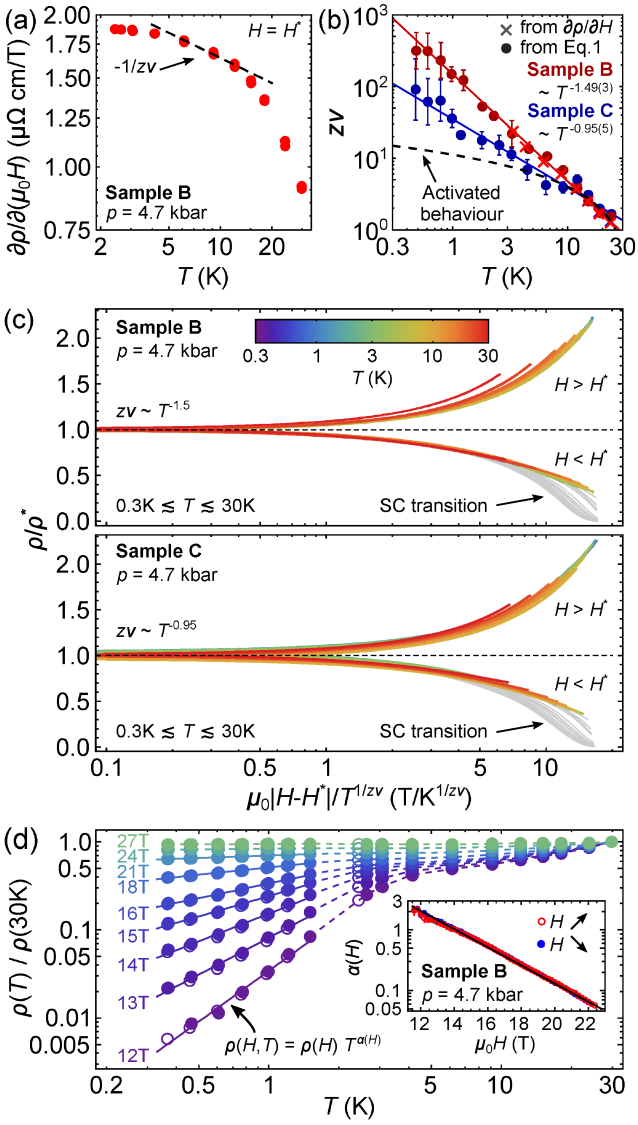

FIG. 3. (a) Log-log plot of the first derivative at the crossing field $H^\star$ (refer to Fig. 2(e)). Error bars are smaller than the symbol size. The slope of the dashed line corresponds to $1/z\nu(T)$. (b) Temperature dependence of $z\nu$ extracted from panel A (crosses) and from the piece-wise extraction shown in the SM (dots) [29]. Error bars indicate a 1σ confidence interval. (c) Scaled magnetotransport data using $z\nu \sim T^{-1.5}$ (sample B) and $z\nu \sim T^{-0.95}$ (sample C). The superconducting transitions (SC) deviate from this scaling form. (d) The low-field, low-temperature resistivity in the mixed state follows a power-law form $\rho(H,T) = \rho(H)T^\alpha$. The inset shows a nearly exponential decay of $\alpha(H)$. For $\mu_0 H > 22\,\mathrm{T}$ the analysis becomes unreliable, and for $\mu_0 H > 28\,\mathrm{T}$, the exponent turns negative. All reported data are measured at $p = 4.7\,\mathrm{kbar}$.

below $T \approx 5$–$10\,\mathrm{K}$ which coincides with a re-entrance of Fermi liquid behavior, Fig. 2(b). This suggests a suppression of order parameter fluctuations due to a finite coupling with the lattice, or a dimensional crossover induced by a changing Fermi surface topology [27, 31, 33, 43].

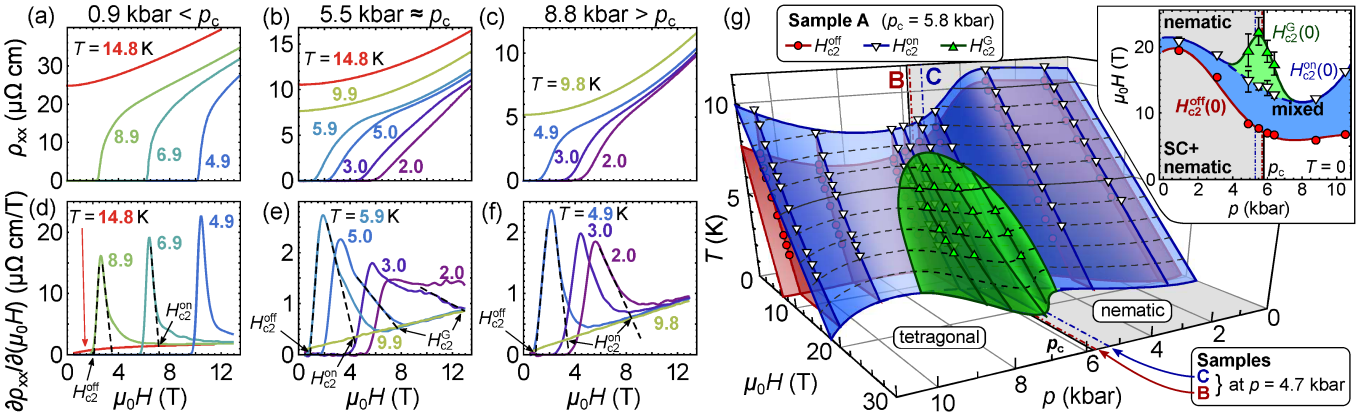

FIG. 4. Evolution of superconductivity for sample A. (a)-(c) Magnetoresistivity and (d)-(f) the corresponding first derivatives showing the development of the superconducting transition in magnetic fields for pressures across the nematic quantum phase transition. (g) Three-dimensional H-p-T superconducting phase diagram. The inset shows the extrapolated critical fields, $H_{c2}^{\rm off}$, $H_{c2}^{\rm on}$ and $H_{c2}^{\rm G}$, defined in panels (d)-(f), in the zero-temperature limit. The relative positions of samples B and C under a pressure of 4.7 kbar in the phase diagram are indicated by dashed and the dotted lines, respectively (see also Figs. 2 and 3). Error bars indicate a 1σ confidence interval.

We now focus on the nature of the underlying phases separated by $H^\star$. Figure 3(d) shows that for fields smaller than $H^\star$, the resistivity within the superconducting mixed state follows a power-law form $\rho \propto T^{\alpha(H)}$ over almost one decade in temperature. We attribute this power-law form to a disordered vortex-liquid phase that freezes into a vortex-glass in the zero-temperature limit, as found in underdoped cuprates [25]. Crossing over into the high-field regime above $H^\star$ where quantum oscillations are present, the resistivity reflects the behavior of a metallic phase with a partial charge-carrier localization, as discussed in the SM [29].

To elucidate the origin and extend of the low-field disordered vortex phase, we investigate the pressure dependence of the superconducting to normal transitions in magnetic fields on sample A ($p_c \approx 5.8$ kbar [27]). Figure 4(a)-(f) shows the magnetoresistivity and its derivative up to 13.5 T inside the nematic phase (0.9 kbar), close to the nematic quantum phase transition (5.5 kbar) and within the tetragonal phase (8.8 kbar). In the nematic and tetragonal phases, the normal-to-superconducting transition widths are nearly temperature and field independent. In contrast, a visible broadening of the transition is found close to p_c, but only for high fields and at low temperatures, thus coinciding with the vortex-liquid phase in sample B. To quantify this additional broadening, we extract the superconducting offset and onset critical fields, $H_{c2}^{\rm off}$ and $H_{c2}^{\rm on}$, as shown in Fig. 4(d)-(f). Furthermore, we define a critical magnetic field $H_{c2}^{\rm G}$, where the magnetoresistivity derivative has an additional shoulder before it returns to its high-temperature normal state background, which is observable only in the vicinity of p_c (Fig. 4(e)). Figure 4(g) summarizes all extracted critical fields and their zero-temperature extrapolations, see also the SM [29]. Interestingly, the zero-temperature superconducting transition width peaks at the nematic quantum phase transition, doubling the extent of the superconducting mixed state. The width of the $H_{c2}^{\rm G}(0)$ peak in pressure is estimated to be $\sigma_p \approx 0.7(2)$ kbar, which agrees well with an estimate for the pressure range of the quantum Griffiths phase, as discussed below. Figure 4(g) also shows that the zero-field superconducting transition does not display any similar broadening. This demonstrates that the peak in $H_{c2}^{\rm G}$ is a low-temperature and high-field effect, ruling out effects of possible pressure inhomogeneities [29].

Discussion Quantum Griffiths phases were previously detected in inhomogeneous superconductor-to-insulator transitions in thin films, including FeSe [19–26]. Here, in bulk $FeSe_{0.89}S_{0.11}$, the situation is very different. The scaling relation only describes the normal state resistivity and holds for magnetic fields up to 45 T and temperatures up to 30 K, vastly exceeding the bulk superconducting phase. We therefore propose that the quantum Griffiths phase in $FeSe_{0.89}S_{0.11}$ emerges from the suppression of the nematic phase with pressure [27, 30, 44] and the formation of rare nematic islands in a tetragonal matrix due to the random distribution of sulfur atoms (Fig. 1), as suggested before (see the SM to Ref. 5). To demonstrate how this can lead to a quantum Griffiths phase, we sample a random distribution of 11 % S atoms over a square lattice, and average the effective sulfur density $x(r)$ over the experimental quasiparticle mean-free path length $\lambda \approx 350$ Å [27], as shown in Fig. 1(b) and (c). The intrinsic local variation $\Delta x(r) \approx 0.4\%$ (std. dev.) gives rise to regions with higher (lower) S content which have a locally lower (higher) critical pressure $p_c(r)$. This is the prototypical case of random-mass disorder that smears the quantum phase transition over a region $\Delta p_c(r)$. By comparing the reported nematic transition temperatures

from pressure and isoelectronic substitution studies, we estimate $\Delta x(r) \propto \Delta p_c(r) \approx 0.4\,\mathrm{kbar}$ [30, 31, 33, 45]. This estimate is similar to the observed pressure range of a broadened superconducting transition, $\sigma_p = 0.7(2)\,\mathrm{kbar}$. This suggests that the peak in $H_{c2}^{\mathrm{G}}(0)$ occurs either due to enhanced superconducting fluctuations within the nematic islands, and/or superconducting nematic islands below the percolation threshold, which get suppressed at $H^\star$. These effects could also provide a favorable environment for the observed inhomogeneous superconducting vortex phase in the vicinity of the nematic QCP. Finally, we note that the spatial arrangement of the S atoms locally breaks the C_4 symmetry of the lattice and thus introduces random-field effects. In the two-dimensional regime, they may limit the size of the nematic domains, but for weak disorder, the corresponding breakup length is exponentially large [46].

It is rather surprising that $FeSe_{0.89}S_{0.11}$ appears as a clean system where quantum oscillations can be observed at lowest temperatures, and yet signatures of a quantum Griffiths phase are detected as well. Thus, in the vicinity of the electronic nematic quantum phase transition, additional effects must be considered, such as the nematoelastic coupling that quenches the two-dimensional quantum critical nematic fluctuations below a cross-over temperature $T_{\mathrm{FL}} \approx 10\,\mathrm{K}$. As a result, Fermi liquid behavior with finite electronic correlations is restored [27, 31, 33, 43], and the quantum Griffiths phase is cut off, leading to the overly strong divergence of $z\nu$. Additionally, a band with likely 3D character is formed due to a Lifshitz transition of the Fermi surface in the proximity of the nematic QCP [27, 33] which may change the effective dimensionality of the system at low temperatures.

The observation of a quantum Griffiths phase in an iron-based superconductor has a number of important implications and provides new insights into the nature of nematic quantum phase transitions. Most notably, the power-law behavior of $z\nu(T)$ could provide new insights into the dynamics of (quenched) nematic quantum fluctuations. Moreover, our study provides evidence that the quantum Griffiths phase affects the mixed state of the superconducting phase. Alternative systems to search for nematic quantum Griffiths phases are those iron-based superconductors in which nematic and tetragonal phases form over limited compositional ranges around QCPs [31, 33, 47, 48]. Experimental probes include uniaxial strain to suppress nematic fluctuations and hence to tune Griffiths phases [49]; NMR and Raman studies to probe the essential role of lattice disorder [50]; STM studies to follow the formation of nematic islands [51]; specific heat measurements to search for predicted power-law behavior at low temperatures [14, 16, 20, 52]. Thus, we hope that our results will guide further theoretical and experimental research in understanding nematic quantum Griffiths phases.

Acknowledgements We thank R. Fernandes for insightful discussions. This work was mainly supported by the EPSRC (EP/I004475/1, EP/I017836/1). P.R. and A.A.H. acknowledge financial support of the Oxford Quantum Materials Platform Grant (EP/M020517/1). A portion of this work was performed at the National High Magnetic Field Laboratory, supported by NSF Cooperative Agreement DMR-1157490 and the State of Florida. Work in Missouri was supported by the NSF (DMR-1828489). We acknowledge financial support of Oxford University John Fell Fund. A.I.C. acknowledges an EPSRC Career Acceleration Fellowship (EP/I004475/1) and Oxford Centre for Applied Superconductivity for financial support.

* p.reiss@fkf.mpg.de; Current address: Max-Planck Institute for Solid State Research, Stuttgart, Germany
† amalia.coldea@physics.ox.ac.uk

[1] John A Hertz, "Zero- and low-temperature phase transitions and the renormalization group," AIP Conference Proceedings **24**, 298–299 (1975).
[2] John A Hertz, "Quantum critical phenomena," Physical Review B **14**, 1165–1184 (1976).
[3] A J Millis, "Effect of a nonzero temperature on quantum critical points in itinerant fermion systems," Physical Review B **48**, 7183–7196 (1993).
[4] Tôru Moriya, *Spin Fluctuations in Itinerant Electron Magnetism*, Springer Series in Solid-State Sciences 56 (Springer-Verlag, Berlin, Heidelberg, New York, Tokyo, 1985).
[5] H.-H. Kuo, J.-H. Chu, J. C. Palmstrom, S. A. Kivelson, and I. R. Fisher, "Ubiquitous signatures of nematic quantum criticality in optimally doped Fe-based superconductors," Science **352**, 958–962 (2016).
[6] Tianbai Cui and Rafael M. Fernandes, "Smeared nematic quantum phase transitions due to rare-region effects in inhomogeneous systems," Physical Review B **98**, 085117 (2018), 1801.01988.
[7] Robert B. Griffiths, "Nonanalytic Behavior Above the Critical Point in a Random Ising Ferromagnet," Physical Review Letters **23**, 17–19 (1969).
[8] Daniel S. Fisher, "Random transverse field Ising spin chains," Physical Review Letters **69**, 534–537 (1992).
[9] Daniel S. Fisher, "Critical behavior of random transverse-field Ising spin chains," Physical Review B **51**, 6411–6461 (1995).
[10] Adrian Del Maestro, Bernd Rosenow, Markus Müller, and Subir Sachdev, "Infinite Randomness Fixed Point of the Superconductor-Metal Quantum Phase Transition," Physical Review Letters **101**, 035701 (2008).
[11] Thomas Vojta, "Disorder-Induced Rounding of Certain Quantum Phase Transitions," Physical Review Letters **90**, 107202 (2003).
[12] Thomas Vojta, "Rare region effects at classical, quantum and nonequilibrium phase transitions," Journal of Physics A: Mathematical and General **39**, R143–R205 (2006), 0602312 [cond-mat].

[13] Thomas Vojta, "Quantum Griffiths Effects and Smeared Phase Transitions in Metals: Theory and Experiment," Journal of Low Temperature Physics **161**, 299–323 (2010).

[14] Sara Ubaid-Kassis, Thomas Vojta, and Almut Schroeder, "Quantum Griffiths Phase in the Weak Itinerant Ferromagnetic Alloy $Ni_{1-x}V_x$," Physical Review Letters **104**, 066402 (2010).

[15] Ruizhe Wang, Adane Gebretsadik, Sara Ubaid-Kassis, Almut Schroeder, Thomas Vojta, Peter J. Baker, Francis L. Pratt, Stephen J. Blundell, Tom Lancaster, Isabel Franke, Johannes S. Möller, and Katharine Page, "Quantum Griffiths Phase Inside the Ferromagnetic Phase of $Ni_{1-x}V_x$," Physical Review Letters **118**, 267202 (2017).

[16] M. C. de Andrade, R. Chau, R. P. Dickey, N. R. Dilley, E. J. Freeman, D. A. Gajewski, M. B. Maple, R. Movshovich, A. H. Castro Neto, G. Castilla, and B. A. Jones, "Evidence for a Common Physical Description of Non-Fermi-Liquid Behavior in Chemically Substituted f-Electron Systems," Physical Review Letters **81**, 5620–5623 (1998).

[17] Daniel Gnida, "Electronic Griffiths phase and quantum interference in disordered heavy-fermion systems," Physical Review B **97**, 081112 (2018).

[18] Xingyu Ji, Yun Zhang, Xiaoying Wang, and Yi Liu, "Griffiths phase-like exponents in the hidden-order state of URu_2Si_2," Journal of Magnetism and Magnetic Materials **519**, 167455 (2021).

[19] Ying Xing, H.-M. Zhang, H.-L. Fu, Haiwen Liu, Yi Sun, J.-P. Peng, F. Wang, Xi Lin, X.-C. Ma, Q.-K. Xue, Jian Wang, and X. C. Xie, "Quantum Griffiths singularity of superconductor-metal transition in Ga thin films," Science **350**, 542–545 (2015).

[20] Yu Saito, Tsutomu Nojima, and Yoshihiro Iwasa, "Quantum phase transitions in highly crystalline two-dimensional superconductors," Nature Communications **9**, 778 (2018).

[21] Nicholas A. Lewellyn, Ilana M. Percher, Jj Nelson, Javier Garcia-Barriocanal, Irina Volotsenko, Aviad Frydman, Thomas Vojta, and Allen M. Goldman, "Infinite-randomness fixed point of the quantum superconductor-metal transitions in amorphous thin films," Physical Review B **99**, 054515 (2019).

[22] Yi Liu, Ziqiao Wang, Pujia Shan, Yue Tang, Chaofei Liu, Cheng Chen, Ying Xing, Qingyan Wang, Haiwen Liu, Xi Lin, X. C. Xie, and Jian Wang, "Anomalous quantum Griffiths singularity in ultrathin crystalline lead films," Nature Communications **10**, 3633 (2019).

[23] G. T. Seidler, T. F. Rosenbaum, and B. W. Veal, "Two-dimensional superconductor-insulator transition in bulk single-crystal $YBa_2Cu_3O_{6.38}$," Physical Review B **45**, 10162–10164 (1992).

[24] R. Schneider, A. G. Zaitsev, D. Fuchs, and H. v. Löhneysen, "Superconductor-Insulator Quantum Phase Transition in Disordered FeSe Thin Films," Physical Review Letters **108**, 257003 (2012).

[25] Xiaoyan Shi, Ping V. Lin, T. Sasagawa, V. Dobrosavljević, and Dragana Popović, "Two-stage magnetic-field-tuned superconductor-insulator transition in underdoped $La_{2-x}Sr_xCuO_4$," Nature Physics **10**, 437–443 (2014).

[26] Yen Hsiang Lin, J. Nelson, and A. M. Goldman, "Superconductivity of very thin films: The superconductor-insulator transition," Physica C: Superconductivity and its Applications **514**, 130–141 (2015).

[27] Pascal Reiss, David E. Graf, Amir A. Haghighirad, William Knafo, Loïc Drigo, Matthew Bristow, Andrew J Schofield, and Amalia I. Coldea, "Quenched nematic criticality and two superconducting domes in an iron-based superconductor," Nature Physics **16**, 89–94 (2020).

[28] A. E. Böhmer, V. Taufour, W. E. Straszheim, Thomas Wolf, and P. C. Canfield, "Variation of transition temperatures and residual resistivity ratio in vapor-grown FeSe," Physical Review B **94**, 024526 (2016).

[29] See Supplemental Material at [URL will be inserted by publisher] for further experimental data and analyses.

[30] Li Xiang, Udhara S Kaluarachchi, Anna E Böhmer, Valentin Taufour, Makariy A Tanatar, Ruslan Prozorov, Sergey L Bud'ko, and Paul C Canfield, "Dome of magnetic order inside the nematic phase of sulfur-substituted FeSe under pressure," Physical Review B **96**, 024511 (2017).

[31] M. Bristow, P. Reiss, A. A. Haghighirad, Z. Zajicek, S. J. Singh, T. Wolf, D. Graf, W. Knafo, A. McCollam, and A. I. Coldea, "Anomalous high-magnetic field electronic state of the nematic superconductors $FeSe_{1-x}S_x$," Phys. Rev. Research **2**, 013309 (2020).

[32] M. D. Watson, Takuya Yamashita, Shigeru Kasahara, William Knafo, M Nardone, J Béard, Frédéric Hardy, Alix McCollam, A Narayanan, S. F. Blake, Thomas Wolf, A. A. Haghighirad, Christoph Meingast, A. J. Schofield, H. v. Löhneysen, Yuji Matsuda, A. I. Coldea, and Takasada Shibauchi, "Dichotomy between the Hole and Electron Behavior in Multiband Superconductor FeSe Probed by Ultrahigh Magnetic Fields," Physical Review Letters **115**, 027006 (2015).

[33] Amalia I. Coldea, Samuel F. Blake, Shigeru Kasahara, Amir A. Haghighirad, Matthew D. Watson, William Knafo, Eun Sang Choi, Alix McCollam, Pascal Reiss, Takuya Yamashita, Mara Bruma, Susannah C. Speller, Yuji Matsuda, Thomas Wolf, Takasada Shibauchi, and Andrew John Schofield, "Evolution of the low-temperature Fermi surface of superconducting $FeSe_{1-x}S_x$ across a nematic phase transition," npj Quantum Materials **4**, 2 (2019).

[34] D Shoenberg, *Magnetic oscillations in metals* (Cambridge University Press, Cambridge, 1984).

[35] I. Paul and M. Garst, "Lattice Effects on Nematic Quantum Criticality in Metals," Physical Review Letters **118**, 227601 (2017).

[36] Xiaoyu Wang and Erez Berg, "Scattering mechanisms and electrical transport near an Ising nematic quantum critical point," Physical Review B **99**, 235136 (2019).

[37] V. S. de Carvalho and Rafael M Fernandes, "Resistivity near a nematic quantum critical point: Impact of acoustic phonons," Physical Review B **100**, 115103 (2019).

[38] Lucas E. Vieira, Vanuildo S. de Carvalho, and Hermann Freire, "DC resistivity near a nematic quantum critical point: Effects of weak disorder and acoustic phonons," Annals of Physics **419**, 168230 (2019).

[39] Matthew P. A. Fisher, "Quantum phase transitions in disordered two-dimensional superconductors," Physical Review Letters **65**, 923–926 (1990).

[40] Taichi Terashima, Naoki Kikugawa, Andhika Kiswandhi, Eun-Sang Choi, James S. Brooks, Shigeru Kasahara, Tatsuya Watashige, Hiroaki Ikeda, Takasada Shibauchi, Yuji Matsuda, Thomas Wolf, Anna E. Böhmer, Frédéric Hardy, Christoph Meingast, Hilbert v. Löhneysen, Michi-To Suzuki, Ryotaro Arita, and Shinya Uji, "Anomalous

Fermi surface in FeSe seen by Shubnikov-de Haas oscillation measurements," Phys. Rev. B **90**, 144517 (2014).

[41] M Bristow, A. A. Haghighirad, M. D. Watson, P. Reiss, Z. Zajicek, J. Prentice, S. J. Blundell, A. McCollam, and A. I. Coldea, "Multi-band effects and dominant interband pairing responsible for the upper critical fields of bulk fese," in preparation (2020).

[42] Liam S Farrar, Matthew Bristow, Amir A Haghighirad, Alix McCollam, Simon J Bending, and Amalia I Coldea, "Suppression of superconductivity and enhanced critical field anisotropy in thin flakes of FeSe," npj Quantum Materials **5**, 29 (2020).

[43] Amalia I. Coldea, "Electronic nematic states tuned by isoelectronic substitution in bulk $FeSe_{1-x}S_x$," (2020).

[44] Kohei Matsuura, Yuta Mizukami, Y. Arai, Y. Sugimura, N. Maejima, A. Machida, T. Watanuki, T. Fukuda, T. Yajima, Z. Hiroi, K. Y. Yip, Y. C. Chan, Q. Niu, Suguru Hosoi, Kousuke Ishida, K. Mukasa, Shigeru Kasahara, J.-G. Cheng, Swee K Goh, Yuji Matsuda, Yoshiya Uwatoko, and Takasada Shibauchi, "Maximizing T_c by tuning nematicity and magnetism in $FeSe_{1-x}S_x$ superconductors," Nature Communications **8**, 1143 (2017).

[45] Pascal Reiss, Matthew D Watson, Timur K Kim, Amir A Haghighirad, D. N. Woodruff, Mara Bruma, S. J. Clarke, and Amalia I Coldea, "Suppression of electronic correlations by chemical pressure from FeSe to FeS," Physical Review B **96**, 121103(R) (2017).

[46] E. T. Seppälä and M. J. Alava, "Susceptibility and percolation in two-dimensional random field Ising magnets," Physical Review E **63**, 066109 (2001).

[47] A E Böhmer, F Hardy, L Wang, T Wolf, P Schweiss, and C Meingast, "Superconductivity-induced re-entrance of the orthorhombic distortion in $Ba_{1-x}K_xFe_2As_2$," Nature Communications **6**, 7911 (2015).

[48] Suguru Hosoi, Kohei Matsuura, Kousuke Ishida, Hao Wang, Yuta Mizukami, Tatsuya Watashige, Shigeru Kasahara, Yuji Matsuda, and Takasada Shibauchi, "Nematic quantum critical point without magnetism in $FeSe_{1-x}S_x$ superconductors," Proceedings of the National Academy of Sciences **113**, 8139–8143 (2016), 1604.00184.

[49] Michele Ghini, Matthew Bristow, Joseph C. A. Prentice, Samuel Sutherland, Samuele Sanna, A. A. Haghighirad, and A. I. Coldea, "Strain tuning of nematicity and superconductivity in single crystals of FeSe," Physical Review B **103**, 205139 (2021).

[50] Paul Wiecki, Rui Zhou, Marc-Henri Julien, Anna E. Böhmer, and Jörg Schmalian, "Edwards-Anderson parameter and local Ising-nematicity in FeSe revealed via NMR spectral broadening," , 1–9 (2021).

[51] He Zhao, Hong Li, Lianyang Dong, Binjie Xu, John Schneeloch, Ruidan Zhong, Minghu Fang, Genda Gu, John Harter, Stephen D. Wilson, Ziqiang Wang, and Ilija Zeljkovic, "Nematic transition and nanoscale suppression of superconductivity in Fe(Te,Se)," Nature Physics **17**, 903–908 (2021).

[52] A. H. Castro Neto, G Castilla, and B A Jones, "Non-Fermi Liquid Behavior and Griffiths Phase in f-Electron Compounds," Physical Review Letters **81**, 3531–3534 (1998).

Supplemental Material: Signatures of a quantum Griffiths phase close to an electronic nematic quantum phase transition

Pascal Reiss,[1,*] David Graf,[2] Amir A. Haghighirad,[1,3] Thomas Vojta,[4] and Amalia I. Coldea[1,†]

[1] *Clarendon Laboratory, Department of Physics, University of Oxford, Oxford, UK*
[2] *National High Magnetic Field Laboratory, Florida State University, Tallahassee, FL, USA*
[3] *Institute for Quantum Materials and Technologies, Karlsruhe Institute of Technology, Karlsruhe, Germany*
[4] *Department of Physics, Missouri University of Science and Technology, Rolla, MO, USA*

(Dated: September 27, 2021)

This Supplemental Material contains additional data and analysis which enhance the findings presented in the main paper.

Sample variation and pressure dependence

The samples A-C reported in the main manuscript were discussed in a previous study dedicated to quantum oscillations [1]. We mapped out the suppression of the nematic phase in $FeSe_{0.89}S_{0.11}$ for sample A under pressure and identified a critical pressure $p_c = 5.8$ kbar at which the nematic phase is suppressed [1]. Sample A was measured inside a piston cylinder pressure cell in fields up to 13.5T, and the pressure was determined from the superconducting transition of Sn at low temperatures.

In this Letter, we focus on the magnetotransport behavior of samples B and C, which were measured simultaneously in a piston cylinder pressure cell in a hybrid magnet with field sweeps between 11.4-45 T. Here, the applied pressure was determined by means of the Ruby florescence method below 4 K.

Even though all samples originate from the same batch, it is important to note that very small variations in sulfur content are expected to occur between different crystals. This is mainly due to the thermal gradient generated during the chemical vapor growth [2] and hence

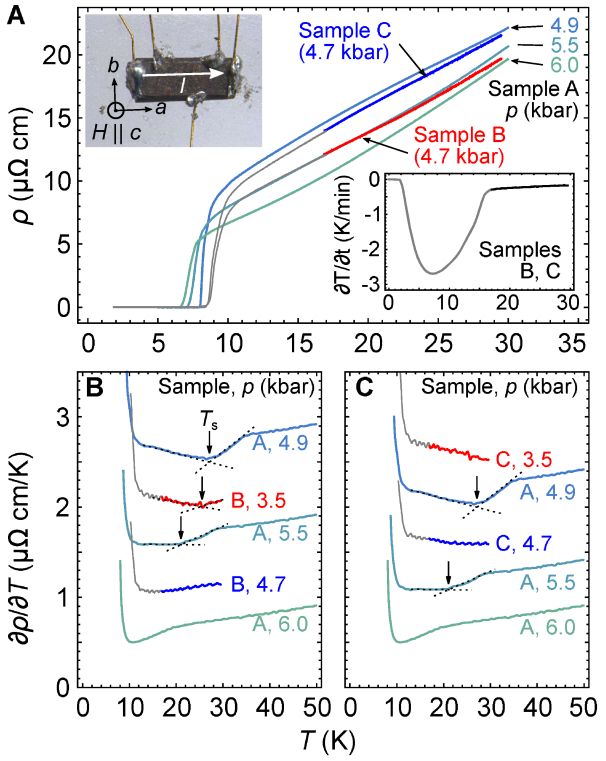

FIG. SM1. (**A**) Temperature dependence of the zero-field resistivity under pressure for samples A, B and C. The lower inset shows a faster cooling rate for samples B and C below 17 K restricting the temperature interval for comparing sample resistivities. Resistivities of samples B and C below 17 K are shown as gray lines. The top inset shows a photograph of sample A, with the tetragonal unit axes a and b and the current direction I indicated. The magnetic field was applied along $H||c$. (**B,C**) First derivative of the zero-field resistivities shown in panel A from which the structural transition temperature T_s can be extracted.

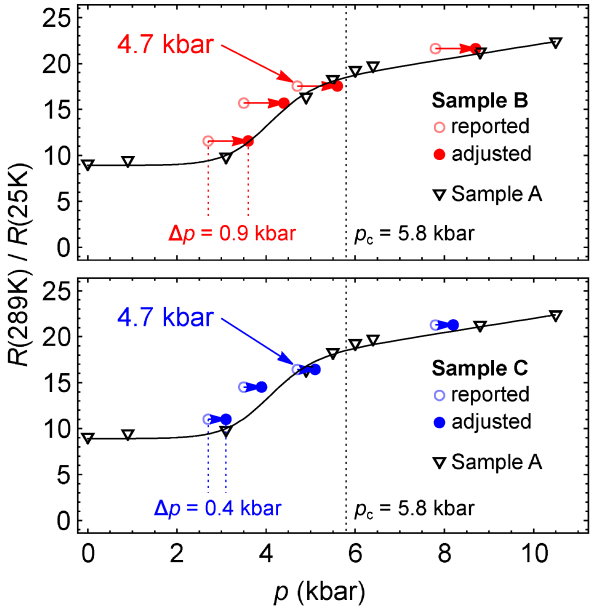

FIG. SM2. Pressure evolution of the residual resistivity ratio (RRR) of samples A, B and C. This ratio, which is a contact-layout independent measure, can be used to estimate the pressure offset for samples B (top) and C (bottom), as indicated by the horizontal arrows.

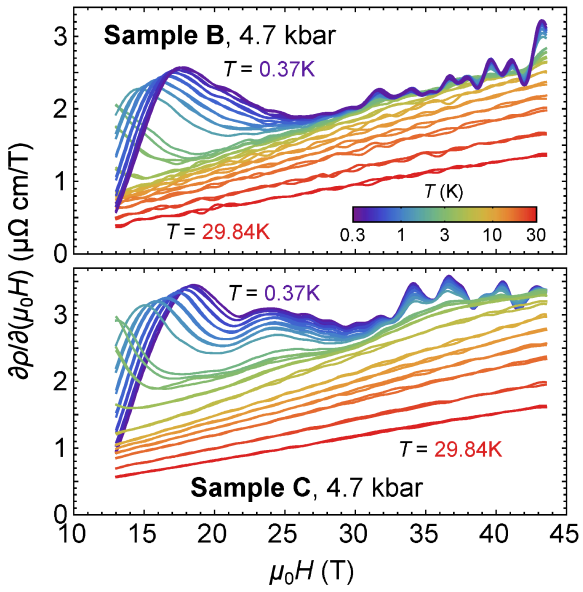

FIG. SM3. First derivatives of the magnetoresistivity for samples B (top) and C (bottom) at different low temperatures up to 45 T. Note the presence of a strong low-frequency quantum oscillation visible in sample C at low temperatures, but absent in sample B.

a locally varying growth temperature along the ampule which leads to locally varying gas pressures. In order to minimize the sample variation, we screened more than 20 samples in zero field at ambient pressure. We chose to study in detail the cleanest samples with the largest residual-resistivity ratio from transport measurements with a similar nematic transition temperature. All single crystals used naturally grew as platelets with well defined facets along the tetragonal unit axes, with the crystallographic c axis perpendicular. The inset to Figure SM1A shows a photograph of sample A. Electrical contacts were attached such that the current was applied along the tetragonal a axis. For all studies, the magnetic field was applied along the c axis. Note that in the nematic phase, the unit cell rotates by 45° along c.

In order to compare all samples, and to estimate their proximity to the nematic quantum phase transition, we use the pressure scale established for sample A, where the nematic quantum phase transition occurs for 5.8 kbar [1]. A "pressure correction" is applied for samples B and C based on their low-temperature resistivity dependencies, in order to account for varying sulfur contents. We note that the nematic phase is suppressed both with pressure and with increasing sulfur content and hence we expect that a higher sulfur content leads to a reduction of the critical pressure. Fig. SM1A show the resistivity versus temperature for all samples A-C. Evidently, the low-temperature resistivity is suppressed with increasing pressure, as shown for sample A. The resistivity of Sample B at 4.7 kbar traces almost exactly the cooling curve of sample A at 5.5 kbar, leading to a first pressure correction $\Delta p_B \approx 0.8$ kbar whereas for sample C, $\Delta p_C \approx 0.5$ kbar. The resistivity derivatives as a function of temperature can be used to extract the structural transition temperature T_s, as demonstrated in Fig. SM1B and C. These results suggests that T_s of sample B at 3.5 kbar is similar to that of sample A at 4.9 kbar, which would correspond to a pressure offset of $\Delta p_B \gtrsim 1.4$ kbar. Furthermore, at 4.7 kbar (sample B) no transition can be resolved, suggesting $\Delta p_B \gtrsim 1.2$. For sample C, we cannot deduce a definitive pressure correction as no transition could be resolved, which are likely to occur at higher temperatures. Nevertheless, we can infer an upper limit $\Delta p_C < 0.8$ kbar.

Another method to compare the pressure evolution of samples A-C is to compare their residual resistivity ratios (RRR) between the room temperature resistivity and that at the onset of superconductivity. Determining the pressure offset from RRR has the added benefit, in comparison to the absolute resistivity (Fig. SM1A) that it is insensitive to uncertainties in the contact layout. RRR of sample A increases substantially as the nematic phase is suppressed, and almost doubles between zero pressure and p_c, as shown in Fig. SM2. The best match of the RRR values between sample A and those of samples B and C, is achieved if one assumes pressure offsets of $\Delta p_B \approx 0.9$ kbar and $\Delta p_C \approx 0.4$ kbar, respectively.

Next, we directly address the position of each sample in the nematic phase diagram. The disappearance of a low-frequency quantum oscillation frequency has been previously interpreted as a Lifshitz transition which occurs at the nematic quantum phase transition [1, 3]. A

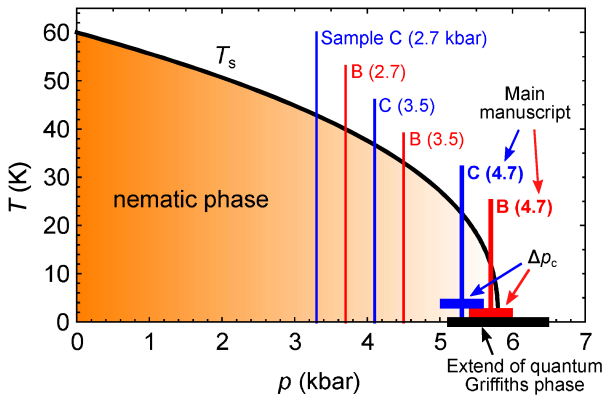

FIG. SM4. Pressure-temperature phase diagram of $FeSe_{0.89}S_{0.11}$. The position of samples B and C within the nematic phase based on sample A is indicated as a function of the reported pressure. These variations for high quality single crystals from the same batch occur due to the small variation in Se/S ratio. The horizontal bars indicate the pressure uncertainty due to the pressure correction for sample B and C (red, blue), and the experimental pressure range of the quantum Griffiths phase, as discussed in the main manuscript.

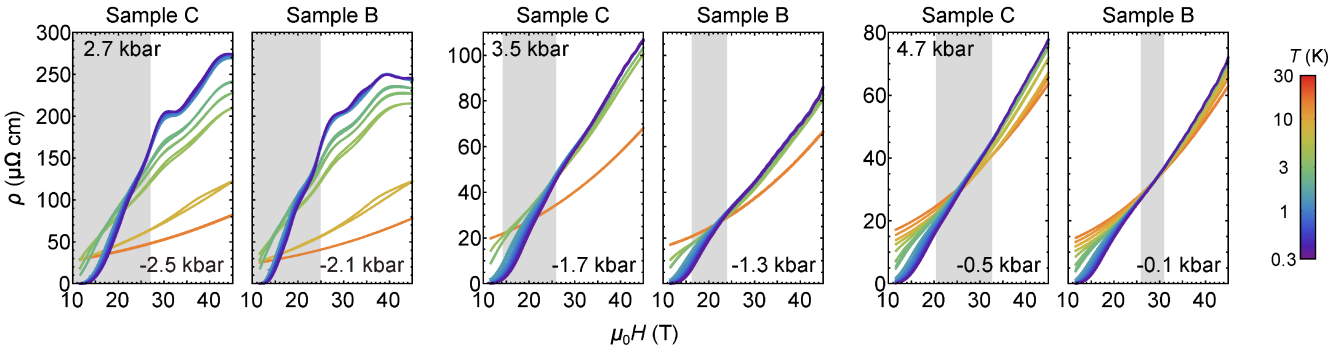

FIG. SM5. Pressure evolution of the magnetoresistivity crossing in samples B and C for temperatures $T \lesssim 15\,\mathrm{K}$. The shaded area marks the field range over which crossings can be observed. Pressures given in the top-left corner indicate the measured value, whereas the pressure value given in the bottom-right corner indicate the distance to the nematic quantum phase transition.

low-frequency quantum oscillation is clearly present for sample C, but absent in sample B at 4.7 kbar, as shown in the first derivative of the magnetoresistivity in Fig. SM3. Hence, we can infer that sample C is still within the nematic phase at 4.7 kbar, whilst sample B is at the nematic quantum phase transition (within experimental pressure resolution).

Based on all these different approaches, our best estimates for the pressure offsets in samples B and C, which we attribute to small variations in the sulfur content, are as follows:

$$\Delta p_{\mathrm{B}} \approx (1.0 \pm 0.3)\,\mathrm{kbar} \quad (1)$$

$$\Delta p_{\mathrm{C}} \approx (0.6 \pm 0.3)\,\mathrm{kbar} \quad (2)$$

These pressure offsets mark the position of samples B and C under pressure within the nematic phase, having sample B at $p = 4.7\,\mathrm{kbar}$ basically located at the nematic quantum phase transition, (within experimental uncertainty) as shown in Fig. SM4.

Evolution of the magnetoresistivity crossing with pressure in different samples

Fig. SM5 shows the magnetoresistivity data for samples B and C as a function of temperature and pressure up to $p = 4.7\,\mathrm{kbar}$ using common temperature range for all pressures $0.3\,\mathrm{K} \lesssim T \lesssim 15\,\mathrm{K}$ for a easier comparison. The order of the panels in Fig. SM5 corresponds to their relative position within the nematic phase as determined from Fig. SM4. With increasing pressure, or equivalently with *decreasing* distance to the nematic quantum phase transition, the field range of magnetoresistivity crossings becomes narrower, and it moves to higher fields (shaded area in Fig. SM5). The crossing collapses to a single point in sample B at 4.7 kbar which is the data set that is extensively discussed in the main paper.

Superconductivity

Figure SM6A shows the temperature and pressure dependence of the critical fields H_{c2}^{off}, H_{c2}^{on} and H_{c2}^{G} describing the offset, onset and additional shoulder of the normal-to-superconductor transitions of sample A (see main paper for their definitions). Also shown are the low-order polynomial fits used to extrapolate the zero-temperature values $H_{c2}^{\mathrm{off}}(0)$, $H_{c2}^{\mathrm{on}}(0)$ and $H_{c2}^{\mathrm{G}}(0)$. A linear polynomial has been used unless the data clearly displays a visible curvature. For a refined error estimate of $H_{c2}^{\mathrm{G}}(0)$, both linear and third order polynomials are shown as well. Importantly, the polynomial order used does not qualitatively change the main finding, i.e. a peak in $H_{c2}^{\mathrm{G}}(0)$ at the nematic quantum critical point, shown in Fig. SM6B and C.

Figure SM7 compares the evolution of the zero-field and of the zero-temperature superconducting transitions as a function of pressure across the nematic quantum phase transition. Panels A and B show that the transitions from the normal to the superconducting phase in zero field and finite temperatures are sharp for all pressures, which rules out effects from possible pressure inhomogeneities. The extracted evolution of T_c^{off} and T_c^{on} with pressure are shown in Panel C. When compared to the evolution of the zero-temperature limits of H_c^{off} and H_c^{on} (Panel D), this shows that the overall suppression of $T_c^{\mathrm{off/on}}$ and $H_{c2}^{\mathrm{off/on}}$ are similar. The marked difference is the emergence of the peak in H_{c2}^{G} which exists only in the low-temperature/high-field limit.

Normal state magnetoresistivity

We estimate the normal zero-field resistivity at low temperature for sample B at 4.7 kbar by extrapolating from the high-field magnetoresistivity data above the onset of superconductivity using a two-band model, as shown in Fig. SM8A. Assuming an electron- and a hole-

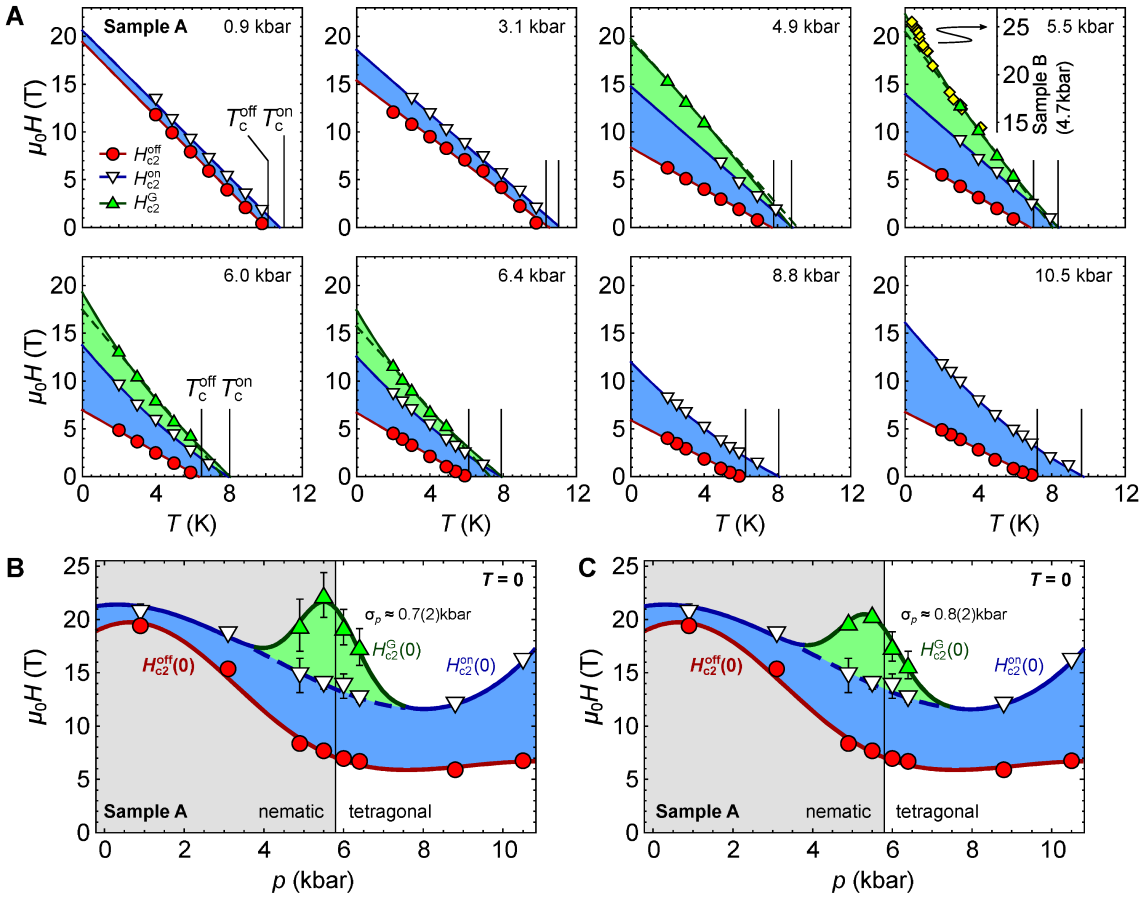

FIG. SM6. **(A)** Temperature and pressure dependence of the critical fields $H_{c2}^{\rm off}$, $H_{c2}^{\rm on}$ and $H_{c2}^{\rm G}$ of sample A. In the panel corresponding to $p = 5.5$ kbar, the onset field of sample B is included for reference (including a vertical offset of 4 T). Solid lines correspond to low-order polynomial fits (typically first order, maximum third order). The dashed lines represent first order fits for comparison. The thin vertical lines indicate $T_c^{\rm off}$ and $T_c^{\rm on}$ extracted from the cooling curves [1]. **(B,C)** Zero-temperature extrapolations $H_{c2}^{\rm off}$, $H_{c2}^{\rm on}$ and $H_{c2}^{\rm G}$ using best fits (B) or linear extrapolations (C) for $H_{c2}^{\rm G}$. The peak in $H_{c2}^{\rm G}$ occurs independently of the fitting function. Panel B shows the same data as the inset of Fig. 4(g) of the main paper.

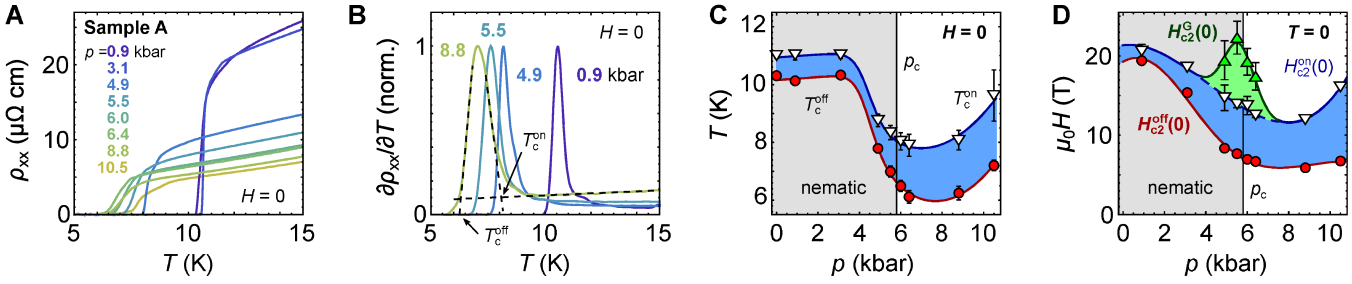

FIG. SM7. Evolution of the zero-field superconducting transition across the nematic quantum phase transition. **(A)** Cool-down resistivity curves across the superconducting transition and **(B)** the normalized derivatives thereof. The transition remains sharp and single-stepped across the nematic quantum phase transition, in contrast to the field-induced transition shown in Fig. 4 of the main paper. **(C)** Pressure dependence of the onset and offset temperatures $T_c^{\rm on}$ and $T_c^{\rm off}$ in zero field. **(D)** Pressure dependence of the onset and offset critical fields $H_{c2}^{\rm on}$, $H_{c2}^{\rm off}$ and $H_{c2}^{\rm G}$ extracted in the zero-temperature limit (identical to the inset of Fig. 4(g)) of the main paper.

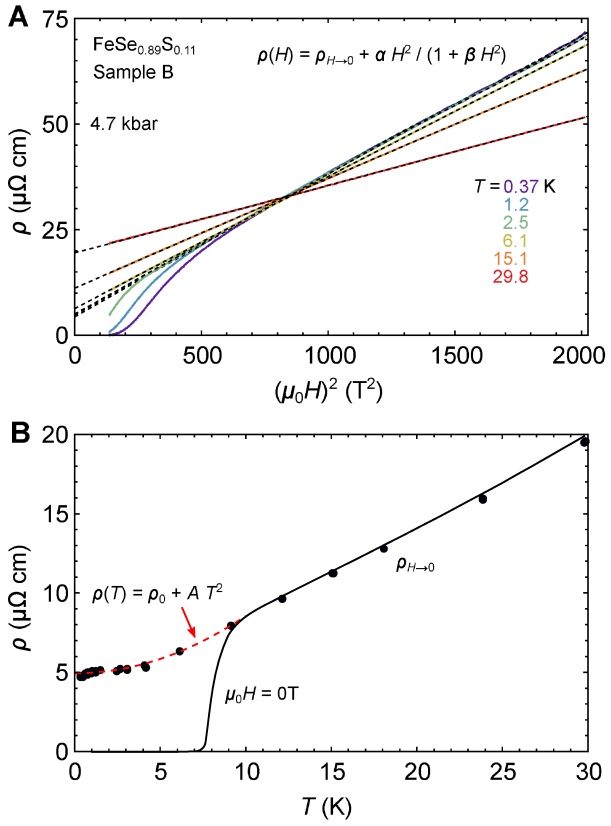

FIG. SM8. (**A**) A two-band model is used to describe the magnetoresistivity data above the onset of superconductivity. (**B**) The extrapolated zero-field resistivity, $\rho_{H\to 0}$, are obtained from the fits in panel A (dots) and the zero-field resistivity data is shown by the solid line. The red dashed line is a fit to the Fermi liquid behavior, $\rho_0 + AT^2$ at low temperatures with $\rho_0 \approx 4.9\,\mu\Omega\,\mathrm{cm}$ and $A \approx 0.036\,\mu\Omega\,\mathrm{cm/K^2}$. Deviations below $T \approx 2\,\mathrm{K}$ are caused by the presence of quantum oscillations at high fields. Panel B is reproduced from Fig. 2(d) of the main paper for reference.

like band with charge carrier densities and mobilities n_e, n_h, μ_e, μ_h, respectively, the magnetoresistivity is given by

$$\rho(B) = \frac{(\mu_e n_e + \mu_h n_h) + \mu_e\mu_h\,(\mu_e n_h + n_e \mu_h)\,B^2}{e\,(\mu_e n_e + \mu_h n_h)^2 + e\mu_e^2\mu_h^2\,(n_e - n_h)^2\,B^2} \quad (3)$$

where e is the electron charge. We can re-write the above expression as

$$\rho(B) = \frac{1}{e(\mu_h n_h + \mu_e n_e)} + \frac{\mu_e n_e \mu_h n_h\,(\mu_e + \mu_h)^2\,B^2}{e\,(\mu_e n_e + \mu_h n_h)^3 + e\mu_e^2\mu_h^2\,(n_e - n_h)^2\,(\mu_e n_e + \mu_h n_h)\,B^2} \quad (4)$$

from which we identify the zero-field limit $\rho_{H\to 0} = (e(\mu_h n_h + \mu_e n_e))^{-1}$. Next, we substitute

$$\alpha = \mu_0^2 \frac{\mu_e n_e \mu_h n_h\,(\mu_e + \mu_h)^2}{e\,(\mu_e n_e + \mu_h n_h)^3} \quad (5)$$

$$\beta = \mu_0^2 \frac{\mu_e^2\mu_h^2\,(n_e - n_h)^2}{(\mu_e n_e + \mu_h n_h)^2} \quad (6)$$

and we assume a non-magnetic environment $B = \mu_0 H$ which allows us to write

$$\rho(H) = \rho_{H\to 0} + \frac{\alpha H^2}{1 + \beta H^2}. \quad (7)$$

In this notation, α effectively measures the strength of the magnetoresistivity which depends on the charge carrier densities and their mobilities. Furthermore, β measures the deviations away from a compensated two-band system, i.e. if $n_e = n_h$ then $\beta = 0$. From previous ARPES, quantum oscillation and magnetoresistivity studies, it is well known that ambient pressure $FeSe_{0.89}S_{0.11}$ is a compensated four-band system, which is dominated by two large, nearly compensated bands [1, 3–5]. The above two-band model fit therefore provides a simplified description and we expect $\beta > 0$, effectively encapsulating the contributions from the two smaller bands.

From Fig. SM8A, we find a good description of the data with only minor deviations visible at temperatures below $T \lesssim 2\,\mathrm{K}$ and fields $\mu_0 H \gtrsim 35\,\mathrm{T}$ which we attribute to the appearance of quantum oscillations. The extracted temperature dependence of $\rho_{H\to 0}(T)$ is shown in Fig. SM8B, together with the zero-field cool down resistivity. For temperatures $T \lesssim 10\,\mathrm{K}$ the extracted zero-field resistivity is consistent with Fermi liquid behavior $\rho \sim T^2$, in good agreement with the previously reported low-temperature dependence of sample A [1]. Overall, this confirms that the normal state resistivity is consistent with predictions for a multi-band Fermi liquid.

Temperature dependent scaling of the magnetoresistivity

From Equation 1 in the main manuscript, we can extract the exponent $z\nu$ from the slope of a log-log plot of the derivative of the magnetoresistivity,

$$\log\left[\partial\rho/\partial(\mu_0 H)\right]|_{H=H^\star} = -1/z\nu \log(T) + \mathrm{const}, \quad (8)$$

which is shown in Fig. 3(a) in the main manuscript for temperatures above the onset of quantum oscillations ($\sim 2\,\mathrm{K}$). Consistent results are obtained using a second method in which the scaling relation, Eq. 1, is applied to all curves in fields $H > H_{c2}^{\mathrm{on}}$ over small temperature intervals, which allows us to extract $z\nu$ per interval, as discussed below.

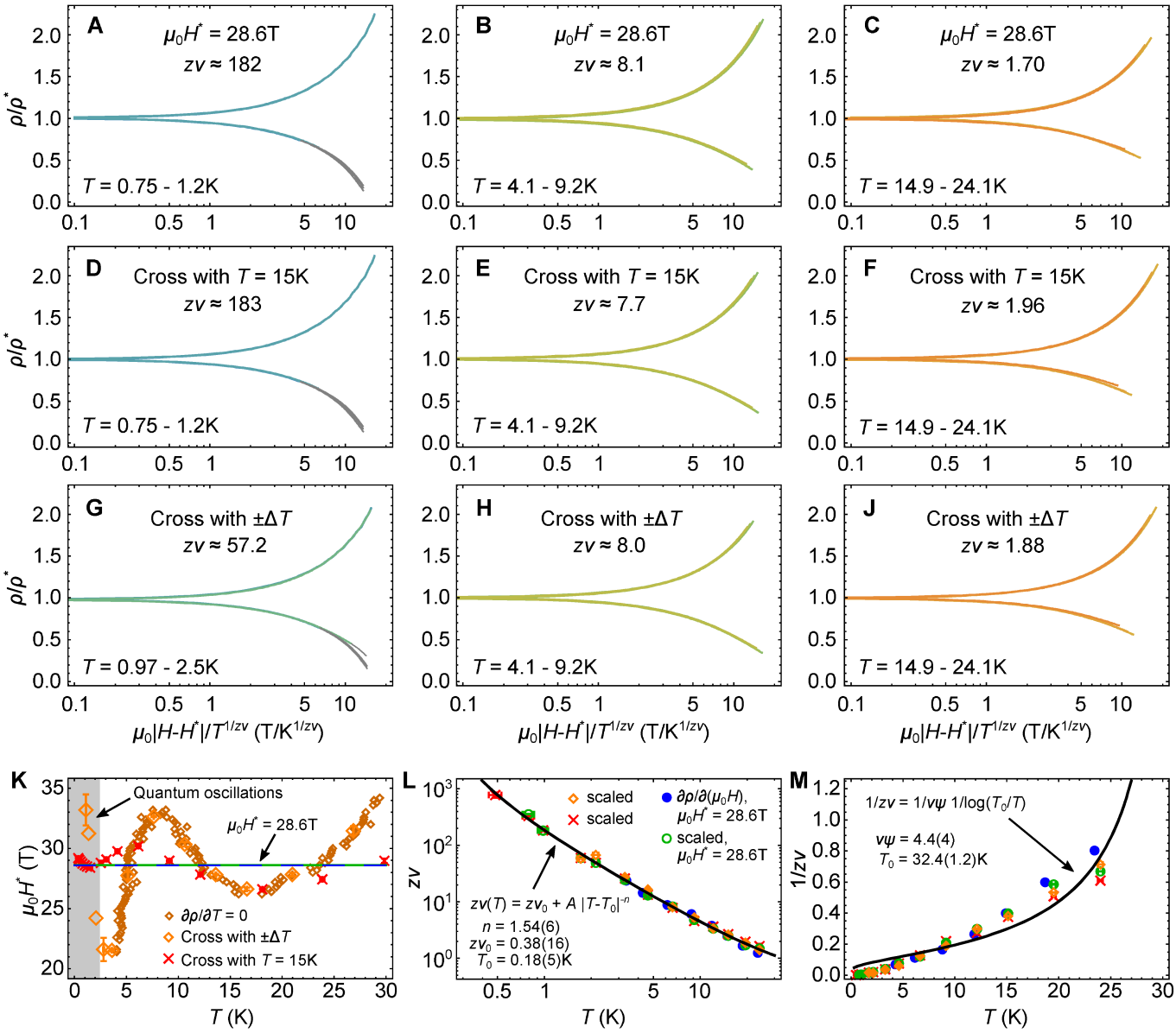

FIG. SM9. **(A)-(J)** Representative examples of the scaling analysis over finite temperature ranges. The spread of the scaled magnetoresistivity data is minimized by varying $z\nu$ as the only parameter. The magnetoresistivity crossing point was either fixed in field $\mu_0 H^\star = 28.6\,\mathrm{T}$ (Panels A-C), obtained from the intersection with the $T = 15\,\mathrm{K}$ dataset (Panels D-F), or from the intersection with neighbouring temperature runs (Panels G-J). **(K)** The temperature dependence of the magnetoresistivity crossing field obtained by the same methods. **(L)** Temperature dependence of $z\nu$. The solid line shows a fit to a generalized power-law form, with the obtained fitting parameters given. **(M)** Same data as in Panel L. The solid line shows a fit assuming activated behavior. Symbols in panels L and M correspond to the same crossing method as indicated in panel K. Errors in panels L and M represent a 1σ confidence interval.

Fig. SM9 shows in detail the scaling analysis of the magnetoresistivity crossing in sample B, which is summarized in the main text. First, the magnetoresistivity over any given temperature range is being rescaled using a manually estimated value for the $z\nu$ parameter (panels A-H). Subsequently, $z\nu$ is obtained by fitting the upper and lower branches independently using a high order polynomial (consistently 7th order, excluding field data below the onset of superconductivity), and then by minimizing the total residual to a global minimum by varying $z\nu$ as the only free parameter. The differences between the panels concern the method how the magnetoresistivity crossing was determined. In Panels A-C, the crossing was set to a constant field $\mu_0 H^\star = 28.6\,\mathrm{T}$ and $\rho^\star = 32.1\,\mu\Omega\,\mathrm{cm}$, consistent with the derivative analysis presented in the main paper (shown as a dashed line in

Panel J). In Panels D-F, the crossing field $H^\star(T)$ is defined as the intersection of the magnetoresistivity at temperature T with the magnetoresistivity at $T \approx 15\,\mathrm{K}$. The advantage of this procedure is that it can be carried out for all temperatures reliably, and the fields obtained are shown in Panel K (crosses). Finally, in Panels G-J, the crossing is defined between two adjacent temperatures measured (shown as large diamonds in Panel K). Equivalently, the crossings are given by tracing the trajectory $\partial\rho/\partial T = 0$ as a function of T and H (shown as small diamonds in Panel K). This method becomes unreliable at lowest temperatures for two reasons: firstly quantum oscillations are not governed by the scaling relation and thus, the true crossing can be masked; secondly, $z\nu$ becomes very large at low-temperatures so that the temperature dependence term in the scaling relation $T^{-1/z\nu}$ becomes effectively constant, and the crossing is smeared by noise.

While the various extraction methods yield different crossing fields in Fig. SM9K, the extracted values for $z\nu$ are only marginally affected (Fig. SM9L). Importantly, the divergence of $z\nu$ towards low temperatures is not influenced by the chosen method. Next, to test for deviations from a pure power-law form at highest or lowest temperatures, we employ a generalized power-law form given by:

$$z\nu(T) = z\nu_0 + A|T - T_0|^{-n} \qquad (9)$$

where $z\nu_0$ describes the high-temperature (i.e. the non-Griffiths) part, and T_0 describes the temperature at which $z\nu$ diverges. Within experimental uncertainty (errors are given as a 1σ confidence interval), $z\nu$ is found to diverge close to zero temperature ($T_0 \approx 0.18(5)\,\mathrm{K}$) (Fig. SM9L). However, the true uncertainty in T_0 is presumably larger than the statistical value obtained from the fit in Panel L. This is because the temperature uncertainty for the $T \approx 370\,\mathrm{mK}$ dataset could be in excess of 40 mK, as the sample inside the cell is away from the outside thermometer. Finally, $z\nu_0$ is consistent with mean-field behavior in the presence of long-range interactions for which $z\nu_0 = 0.5$ [6]. Fig. SM9M shows the best fit of $z\nu(T)$ assuming activated behavior [7], which clearly fails to describe the data, in contrast to the good description assuming power-law behavior (Fig. SM9L).

Extend of the quantum Griffiths phase

Figure SM10 shows the range over which the scaling relation, Eq. 1 of the main manuscript, applies to describe the magnetoresistivity of sample B at a pressure of $p = 4.7\,\mathrm{kbar}$. Evidently, the scaling relation applies to nearly the entire H-T phase space studied. The upper limit marks a crossover from the quantum critical region at low temperatures to the classical region where the scaling form breaks down. The lower limit coincides with the onset of superconductivity, demonstrating that the scaling relation describes the normal (non-superconducting) state.

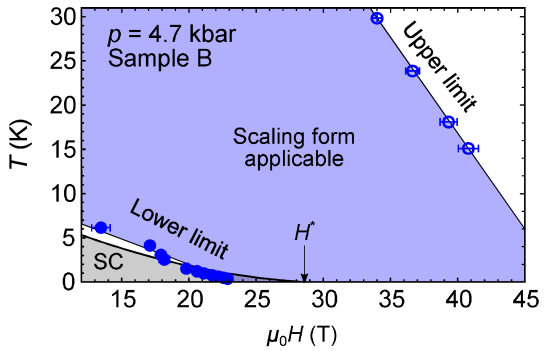

FIG. SM10. Limits of the applicability of the scaling relation, Eq. 1 of the main manuscript, to the magnetoresistivity of sample B at a pressure of $p = 4.7\,\mathrm{kbar}$. At the upper and lower limits, deviations of the scaling form occur. The lower limit coincides with the onset of superconductivity (SC).

Parallel resistor network of mixed phases

In the highest measured magnetic field of $\mu_0 H = 45\,\mathrm{T}$, the resistivity $\rho(T)$ above 10 K displays an approximately exponential increase, characteristic for insulating-like be-

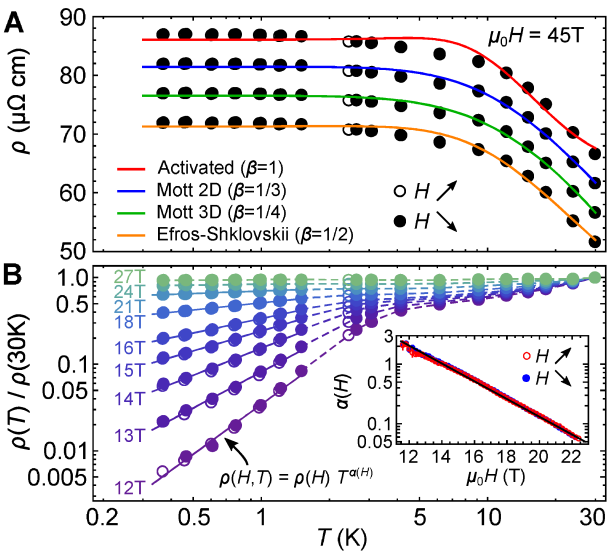

FIG. SM11. High-field and low-field resistivity as function of temperature. (A) In high fields, the data can be described by a phenomenological parallel network of metallic and insulating behavior. Experimental data points and fits are incrementally offset by $+5\,\mu\Omega\,\mathrm{cm}$ for clarity. (B) At low-fields, the resistivity below 2 K follows a power-law form which implies $\rho \to 0$ for $t \to 0$, and $T_c = 0$. The inset shows the nearly exponential field-dependence of the power-law exponent.

havior, as shown in Fig. SM11A. At lower temperatures, a cross-over occurs around 5 K, and $\rho(T)$ saturates below 2 K which is the regime where quantum oscillations become the strongest (Fig. 2 in the main paper). This behavior can be described using a phenomenological model consisting of a parallel network of insulating and metallic conductivities, σ_{ins} and σ_{m}, respectively, given by

$$\sigma_{\mathrm{m}}^{-1}(T) = \rho_0(45\,\mathrm{T}) + AT^2 \tag{10}$$

$$\sigma_{\mathrm{ins}}^{-1}(T) = s\exp((U/k_{\mathrm{B}}T)^{\beta}) \tag{11}$$

$$\rho(T, 45\,\mathrm{T}) = (\sigma_{\mathrm{m}} + \sigma_{\mathrm{ins}})^{-1}. \tag{12}$$

Here, we assume Fermi liquid-like behavior for the metallic part of the conductivity with $A = 0.036\,\mu\Omega\,\mathrm{cm/K}^2$, as obtained for the extrapolated zero-field resistivity shown in Fig. SM8, and which is consistent with previous observations [1]. For the insulating contribution to the total conductivity, U is a characteristic energy scale, and s describes the high temperature conductivity which is lost for $T \to 0$ (k_{B} is the Boltzmann constant). The exponent β depends on the appropriate conduction process and the dimensionality: for activated behavior, $\beta = 1$, whereas variable-range Mott-hoping gives $\beta = 1/(1+d)$ where d is the spatial dimension [8–10]. Including the effects of a Coulomb gap, the Elfros-Shklovskii variable-range hopping leads to $\beta = 1/2$ for all dimensions [11, 12]. Consequently, this phenomenological model gives $\rho(T \to 0, H) = \rho_0(H)$ which ensures a finite metallic conductivity at low temperatures, whereas $\rho(T)$ decays as $\exp(-U/T)$ for higher temperatures, ensuring insulating-like behavior there, as observed in Fig. SM11A. Treating ρ_0, U and s as fitting parameters, we compare the fits of this model for different fixed β to the experimental data in Fig. SM11A. We find that for all values of β, the model broadly captures the temperature dependence of the resistivity observed. We therefore cannot infer which conduction process is the most fitting, but it appears that activated behavior ($\beta = 1$) provides the poorest description. Thus, we speculate that a partial localization might take place in high magnetic fields, reminiscent of the high-field insulating phases of systems where quantum Griffiths phases were observed [7, 13–20].

* p.reiss@fkf.mpg.de; Current address: Max-Planck Institute for Solid State Research, Stuttgart, Germany
† amalia.coldea@physics.ox.ac.uk

[1] Pascal Reiss, David E. Graf, Amir A. Haghighirad, William Knafo, Loïc Drigo, Matthew Bristow, Andrew J Schofield, and Amalia I. Coldea, "Quenched nematic criticality and two superconducting domes in an iron-based superconductor," Nature Physics **16**, 89–94 (2020).

[2] A. E. Böhmer, V. Taufour, W. E. Straszheim, Thomas Wolf, and P. C. Canfield, "Variation of transition temperatures and residual resistivity ratio in vapor-grown FeSe," Physical Review B **94**, 024526 (2016).

[3] Amalia I. Coldea, Samuel F. Blake, Shigeru Kasahara, Amir A. Haghighirad, Matthew D. Watson, William Knafo, Eun Sang Choi, Alix McCollam, Pascal Reiss, Takuya Yamashita, Mara Bruma, Susannah C. Speller, Yuji Matsuda, Thomas Wolf, Takasada Shibauchi, and Andrew John Schofield, "Evolution of the low-temperature Fermi surface of superconducting $FeSe_{1-x}S_x$ across a nematic phase transition," npj Quantum Materials **4**, 2 (2019).

[4] Matthew D Watson, Timur K Kim, Amir A Haghighirad, Samuel F Blake, N R Davies, M Hoesch, Thomas Wolf, and Amalia I Coldea, "Suppression of orbital ordering by chemical pressure in $FeSe_{1-x}S_x$," Physical Review B **92** (2015), 10.1103/PhysRevB.92.121108.

[5] M. Bristow, P. Reiss, A. A. Haghighirad, Z. Zajicek, S. J. Singh, T. Wolf, D. Graf, W. Knafo, A. McCollam, and A. I. Coldea, "Anomalous high-magnetic field electronic state of the nematic superconductors $FeSe_{1-x}S_x$," Phys. Rev. Research **2**, 013309 (2020).

[6] Sebastian Fey, Sebastian C. Kapfer, and Kai Phillip Schmidt, "Quantum Criticality of Two-Dimensional Quantum Magnets with Long-Range Interactions," Physical Review Letters **122**, 017203 (2019), arXiv:1802.06684.

[7] Nicholas A. Lewellyn, Ilana M. Percher, Jj Nelson, Javier Garcia-Barriocanal, Irina Volotsenko, Aviad Frydman, Thomas Vojta, and Allen M. Goldman, "Infinite-randomness fixed point of the quantum superconductor-metal transitions in amorphous thin films," Physical Review B **99**, 054515 (2019).

[8] N. F. Mott, "Conduction in non-crystalline systems," Philosophical Magazine **17**, 1259–1268 (1968).

[9] N. F. Mott, "Conduction in non-crystalline materials," Philosophical Magazine **19**, 835–852 (1969).

[10] N. F. Mott, "Metal-insulator transitions," Pure and Applied Chemistry **52**, 65–72 (1980).

[11] A. L. Efros and B. I. Shklovskii, "Coulomb gap and low temperature conductivity of disordered systems," Journal of Physics C: Solid State Physics **8**, L49–L51 (1975).

[12] A. L. Efros, "Coulomb gap in disordered systems," Journal of Physics C: Solid State Physics **9**, 2021–2030 (1976).

[13] Matthew P. A. Fisher, "Quantum phase transitions in disordered two-dimensional superconductors," Physical Review Letters **65**, 923–926 (1990).

[14] G. T. Seidler, T. F. Rosenbaum, and B. W. Veal, "Two-dimensional superconductor-insulator transition in bulk single-crystal $YBa_2Cu_3O_{6.38}$," Physical Review B **45**, 10162–10164 (1992).

[15] R. Schneider, A. G. Zaitsev, D. Fuchs, and H. v. Löhneysen, "Superconductor-Insulator Quantum Phase Transition in Disordered FeSe Thin Films," Physical Review Letters **108**, 257003 (2012).

[16] Xiaoyan Shi, Ping V. Lin, T. Sasagawa, V. Dobrosavljević, and Dragana Popović, "Two-stage magnetic-field-tuned superconductor-insulator transition in underdoped $La_{2-x}Sr_xCuO_4$," Nature Physics **10**, 437–443 (2014).

[17] Ying Xing, H.-M. Zhang, H.-L. Fu, Haiwen Liu, Yi Sun, J.-P. Peng, F. Wang, Xi Lin, X.-C. Ma, Q.-K. Xue, Jian Wang, and X. C. Xie, "Quantum Griffiths singularity of superconductor-metal transition in Ga thin films," Science **350**, 542–545 (2015).

[18] Yu Saito, Tsutomu Nojima, and Yoshihiro Iwasa, "Quantum phase transitions in highly crystalline two-dimensional superconductors," Nature Communications

9, 778 (2018).

[19] Yi Liu, Ziqiao Wang, Pujia Shan, Yue Tang, Chaofei Liu, Cheng Chen, Ying Xing, Qingyan Wang, Haiwen Liu, Xi Lin, X. C. Xie, and Jian Wang, "Anomalous quantum Griffiths singularity in ultrathin crystalline lead films," Nature Communications **10**, 3633 (2019).

[20] Yen Hsiang Lin, J. Nelson, and A. M. Goldman, "Superconductivity of very thin films: The superconductor-insulator transition," Physica C: Superconductivity and its Applications **514**, 130–141 (2015).